Supporting Information

Mitochondria-targeted artesunate conjugated cyclometalated iridium(III) complexes as potent anti-HepG2 hepatocellular carcinoma agents

Rui-Rong Ye,‡*[a] Wan Peng,‡[a] Bi-Chun Chen,[a] Ning Jiang,[a] Xuan-Qin Chen,[a] Zong-Wan Mao*[b] and Rong-Tao Li*[a]

[a] *Faculty of Life Science and Technology, Kunming University of Science and Technology, Kunming 650500, P. R. China*

[b] *MOE Key Laboratory of Bioinorganic and Synthetic Chemistry, School of Chemistry, Sun Yat-Sen University, Guangzhou 510275, P. R. China.*

* Corresponding author.

E-mail addresses: yerr@mail2.sysu.du.cn (R.-R. Ye), cesmzw@mail.sysu.edu.cn (Z.-W. Mao), rongtaolikm@163.com (R.-T. Li).

‡ These authors contributed equally.

Table of Contents

Scheme S1 Synthetic routes of **Ir-ART-1**, **Ir-ART-2** and **Ir-ART-3**

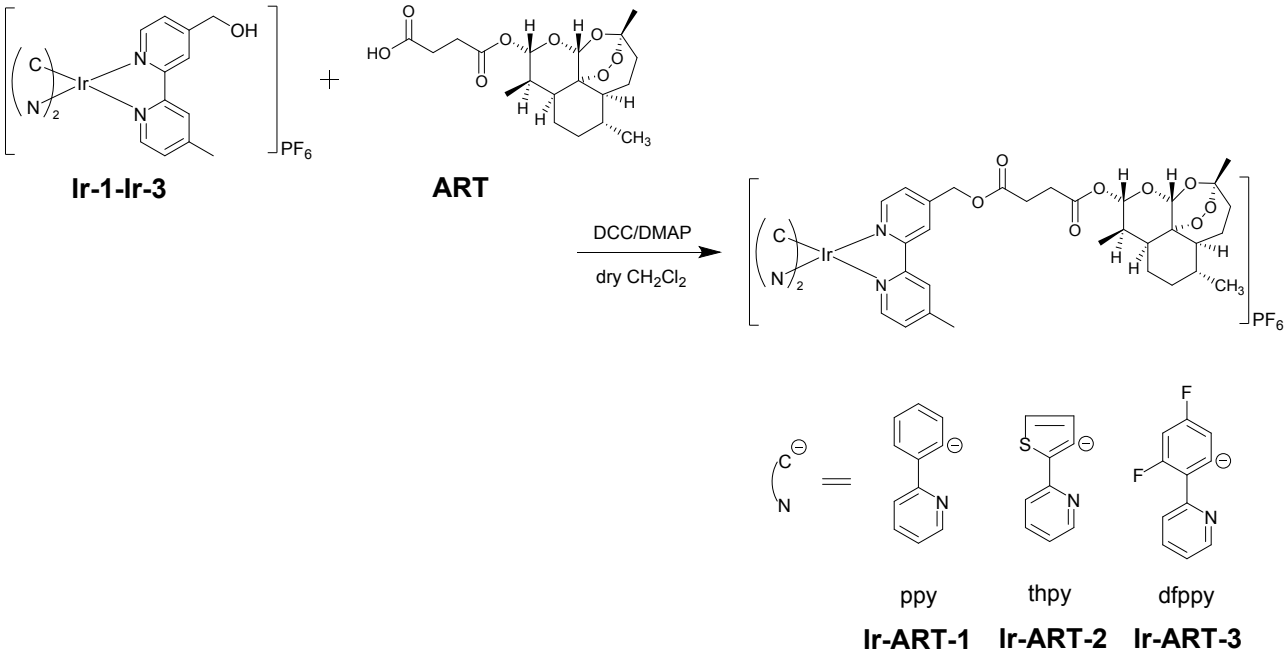

Ir-1-Ir-3 **ART**

Ir-ART-1 **Ir-ART-2** **Ir-ART-3**

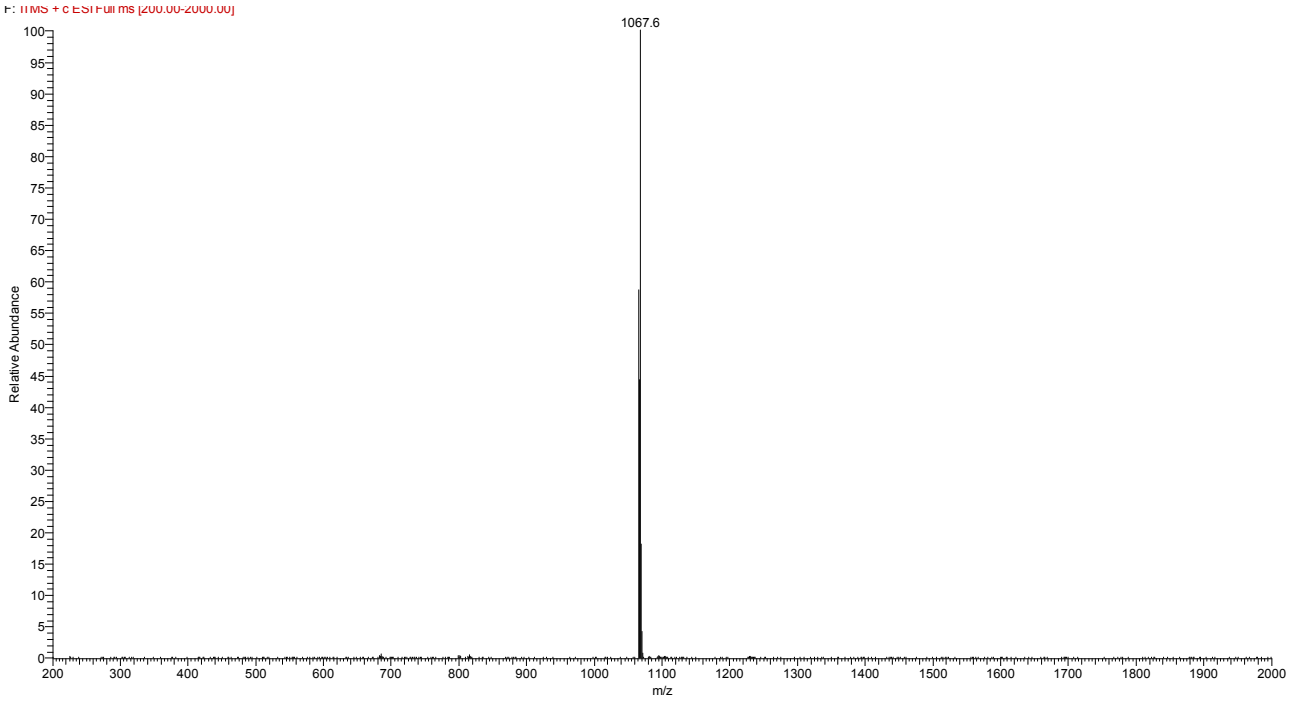

Fig. S1 ESI-MS characterization of **Ir-ART-1**, 1067.6 $[M\text{-}PF_6]^+$.

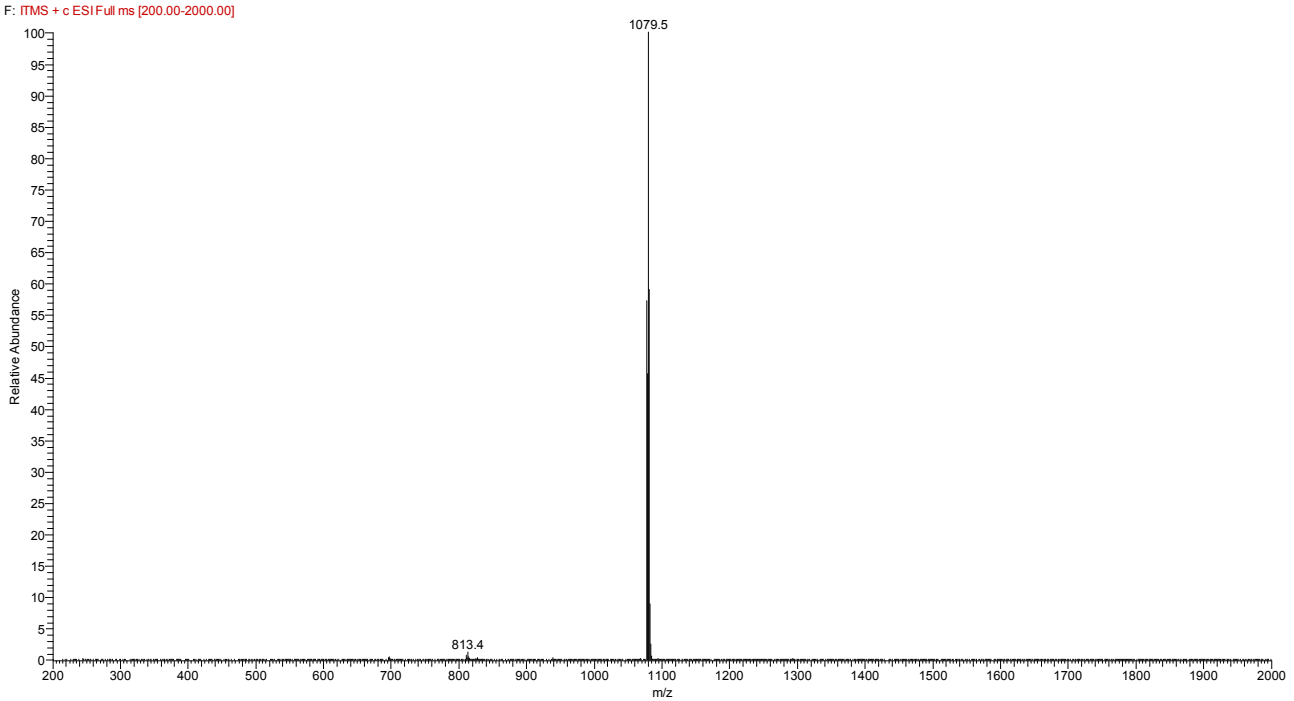

Fig. S2 ESI-MS characterization of **Ir-ART-2**, 1079.5 $[M\text{-}PF_6]^+$.

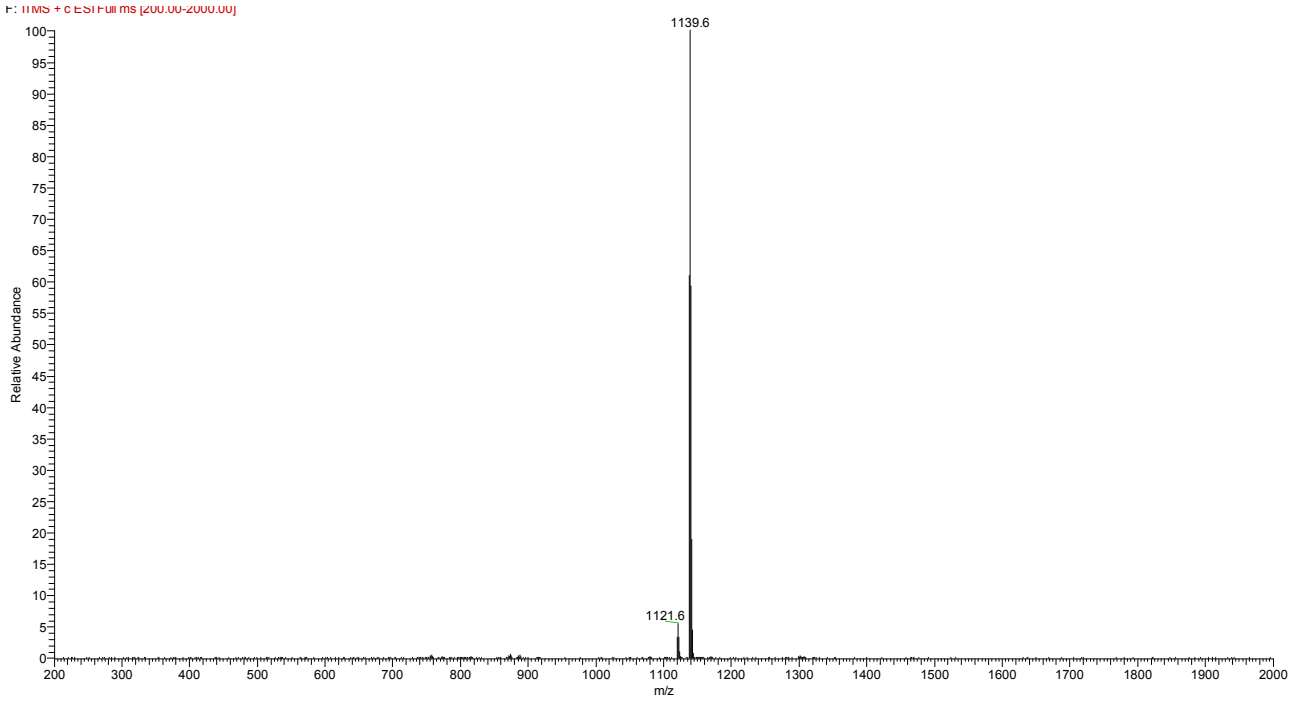

Fig. S3 ESI-MS characterization of **Ir-ART-3**, 1139.6 $[M\text{-}PF_6]^+$.

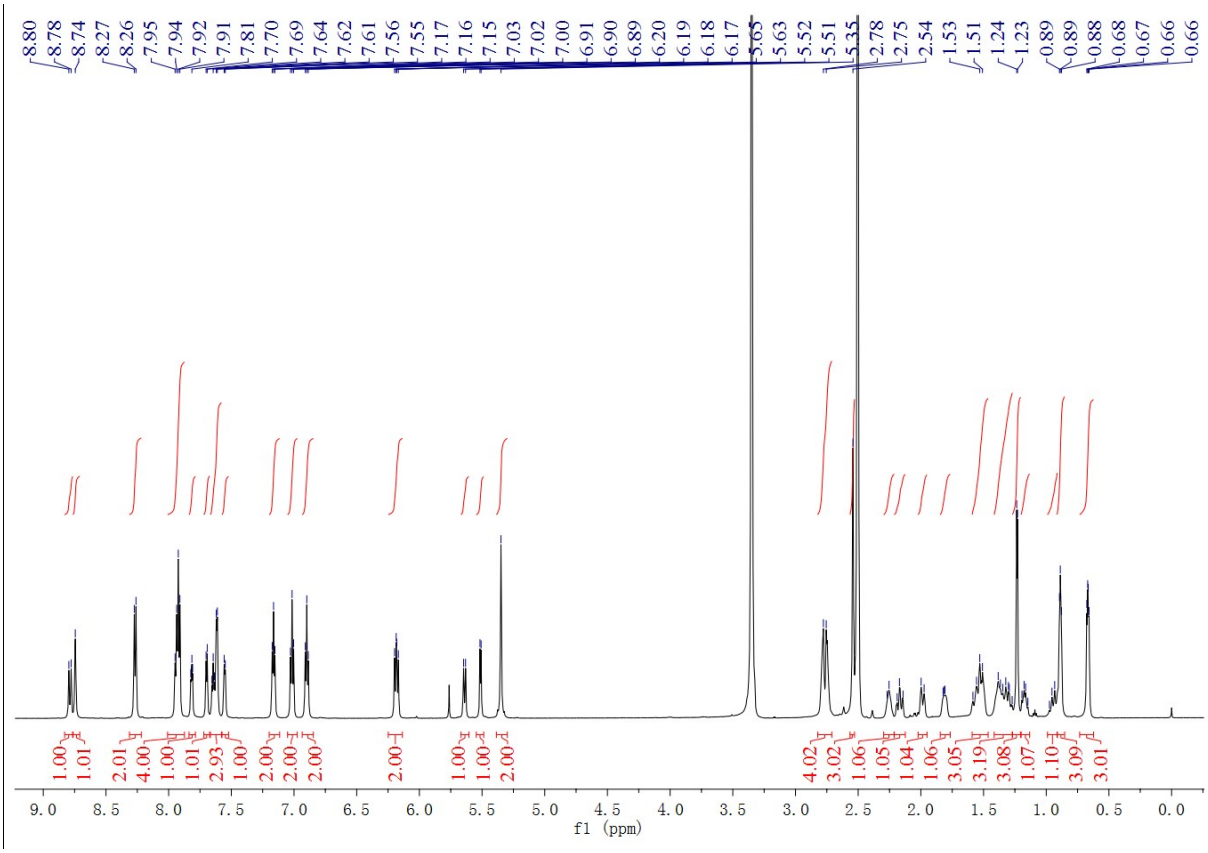

Fig. S4 ^1H NMR spectrum of **Ir-ART-1**.

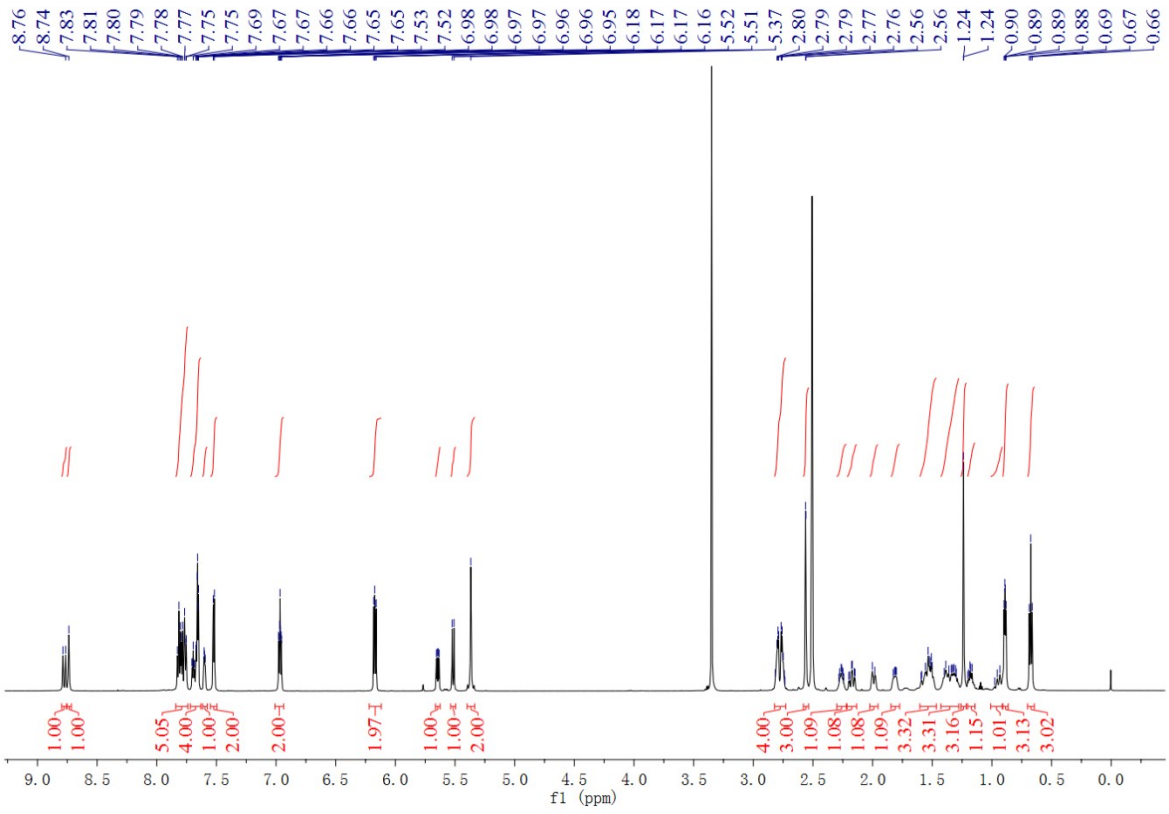

Fig. S5 ^{1}H NMR spectrum of **Ir-ART-2**.

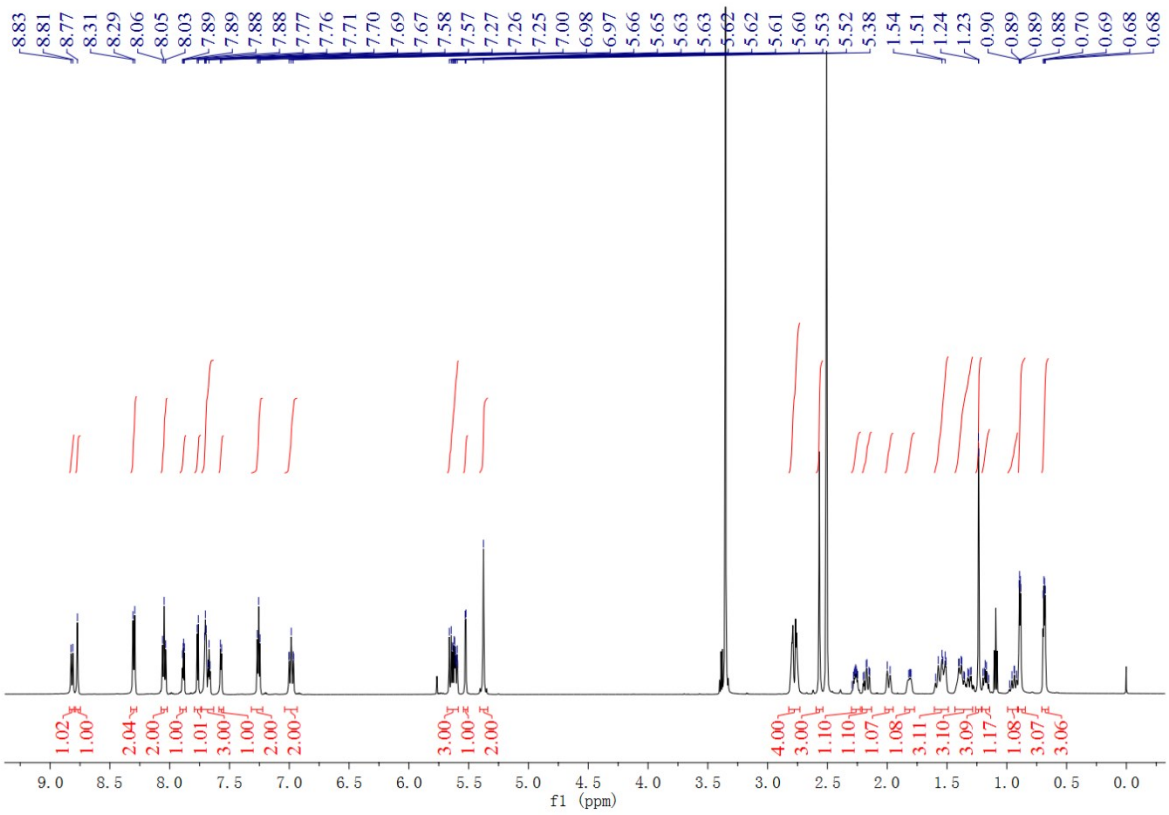

Fig. S6 ^{1}H NMR spectrum of **Ir-ART-3**.

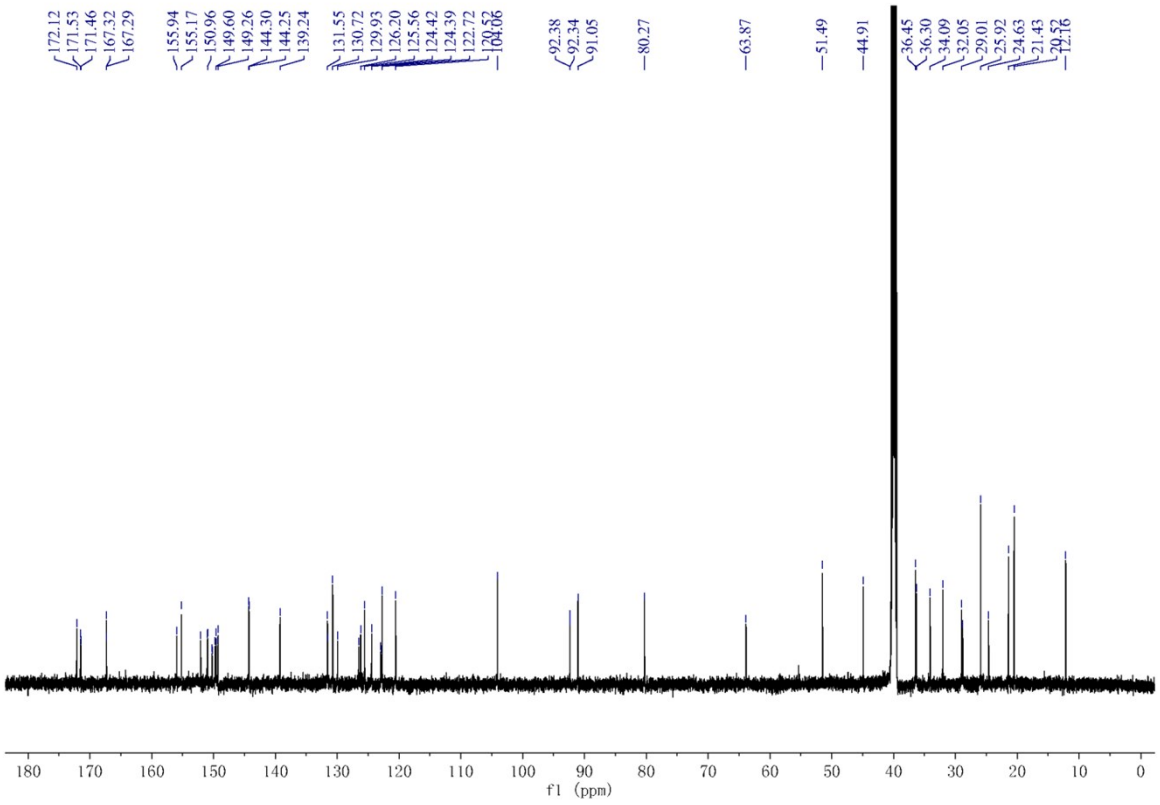

Fig. S7 ^{13}C NMR spectrum of **Ir-ART-1**.

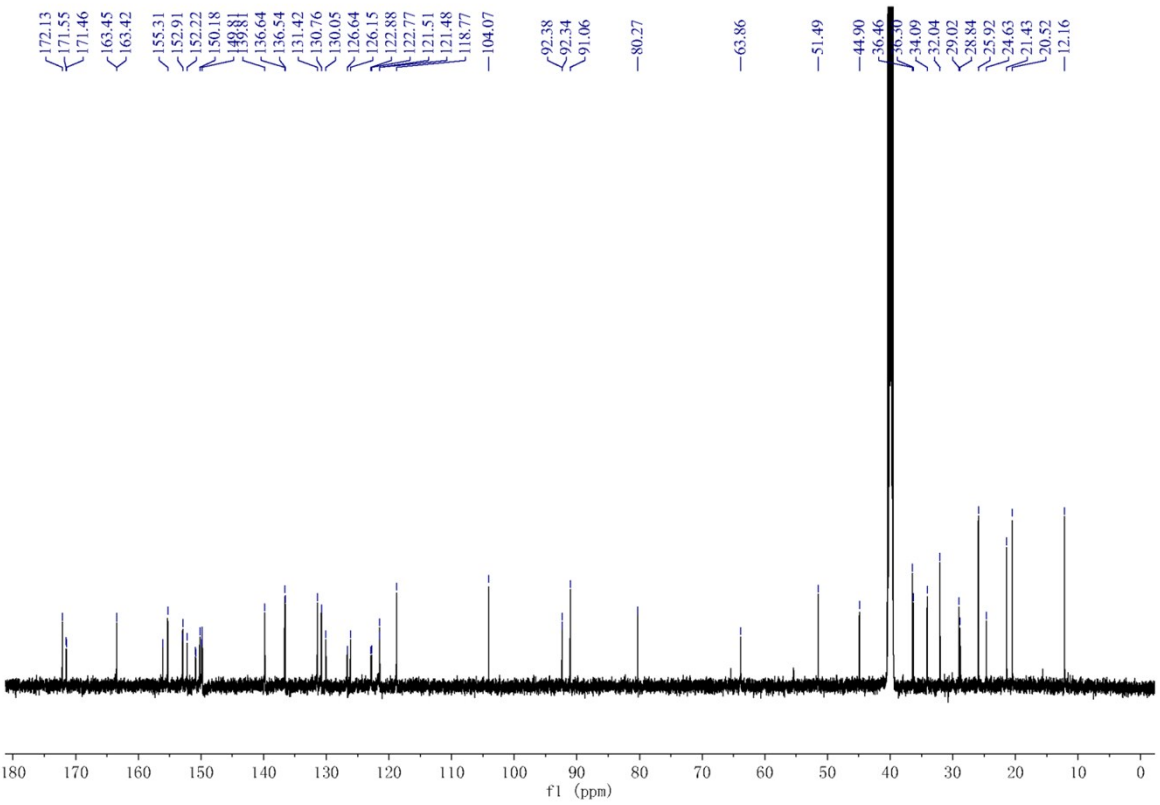

Fig. S8 ^{13}C NMR spectrum of **Ir-ART-2**.

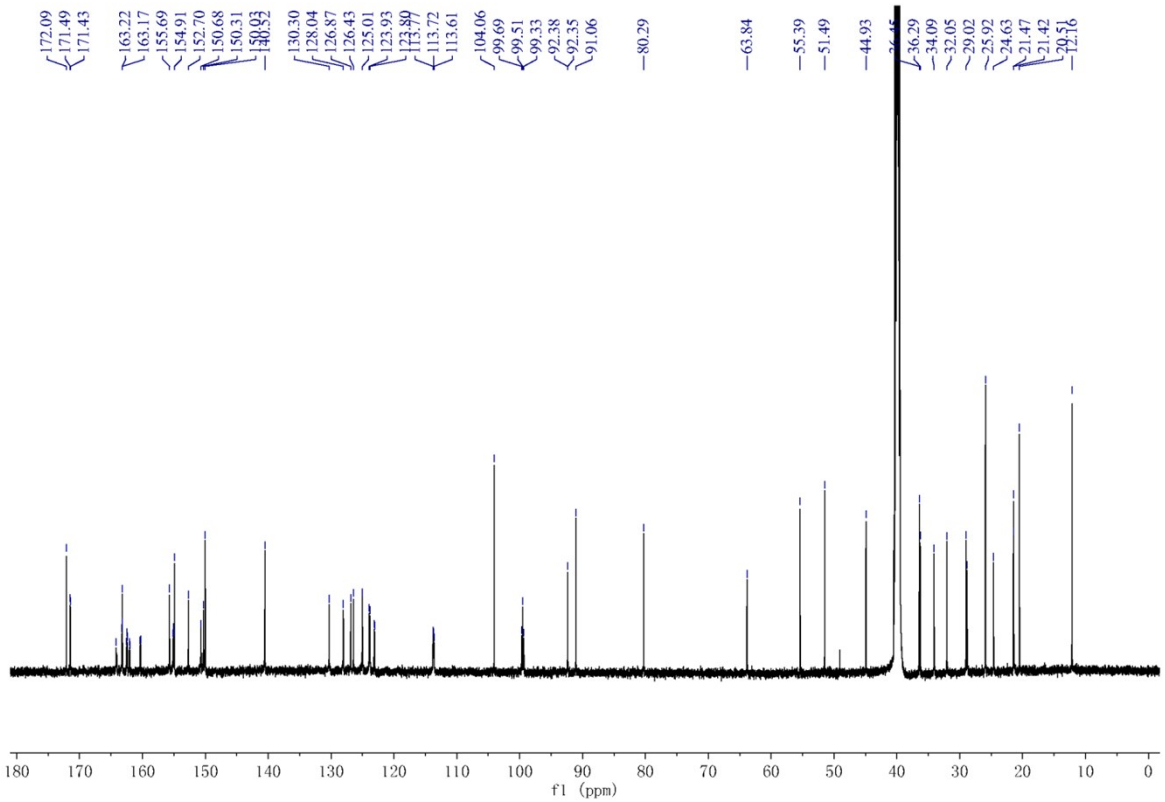

Fig. S9 ^{13}C NMR spectrum of **Ir-ART-3**.

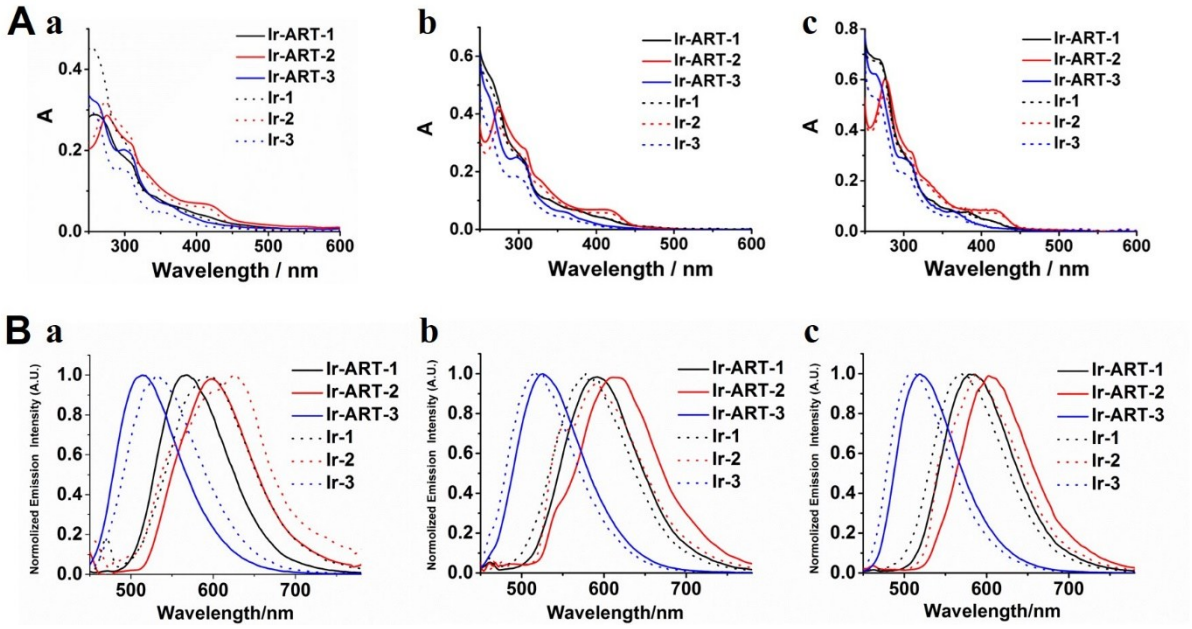

Fig. S10 (A) UV/Vis spectra (1×10^{-5} M) of Ir(III) complexes measured in PBS (a), CH_3CN (b) and CH_2Cl_2 (c) at 298 K. (B) Emission spectra (1×10^{-5} M) of Ir(III) complexes measured in PBS (a), CH_3CN (b) and CH_2Cl_2 (c) at 298 K (λ_{ex} = 405 nm).

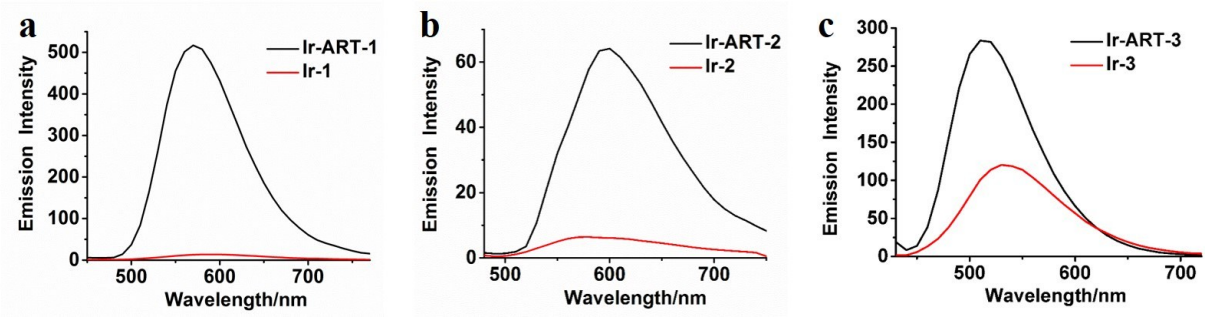

Fig. S11 Emission spectra of 1×10^{-5} M iridium complexes conjugate with (**Ir-ART-1**–**3**) or without (**Ir-1**–**3**) ART in PBS.

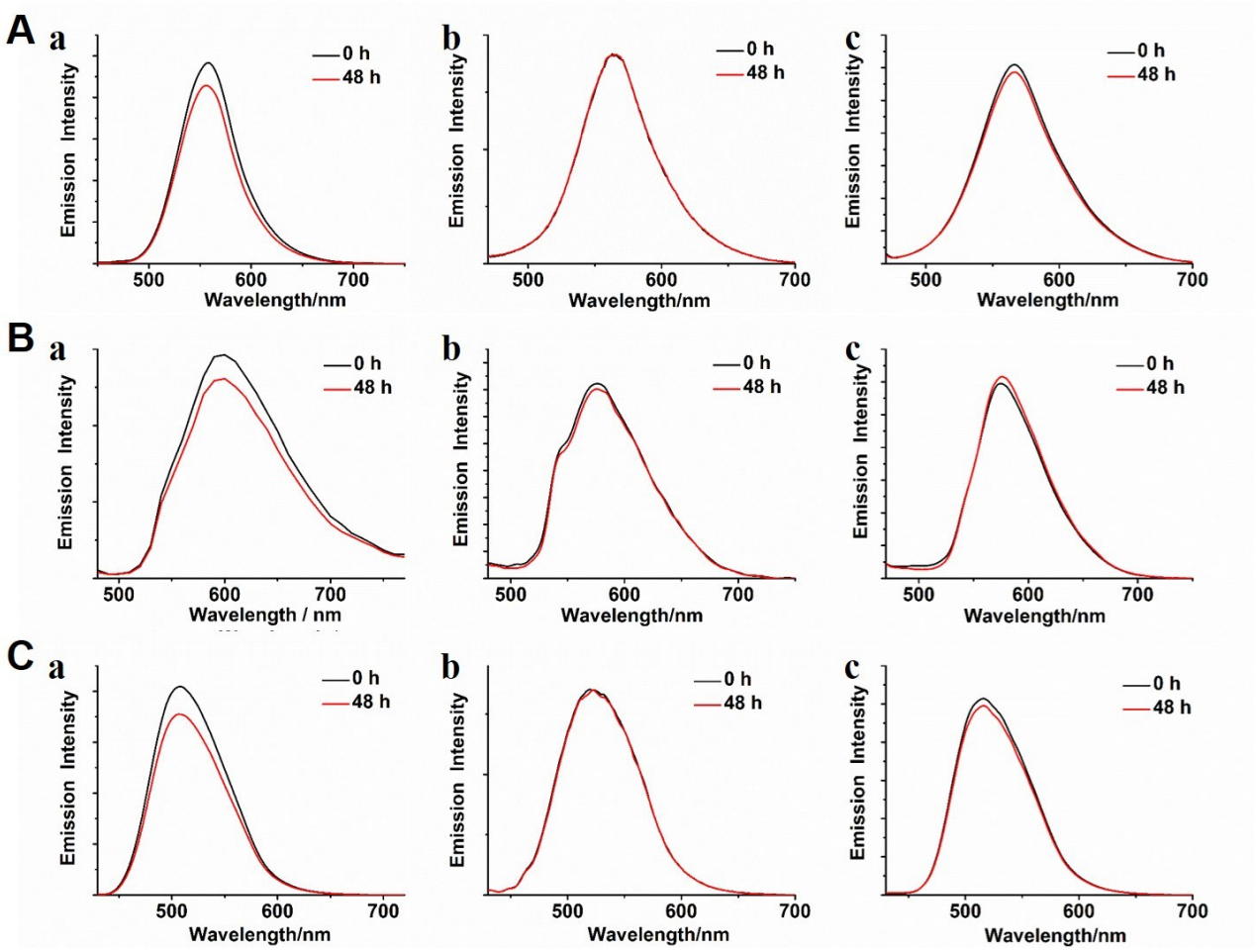

Fig. S12 Emission spectra of **Ir-ART-1** (A), **Ir-ART-2** (B) and **Ir-ART-3** (C) in PBS (a), CH_3CN (b) and CH_2Cl_2 (c) at 0 and 48 h.

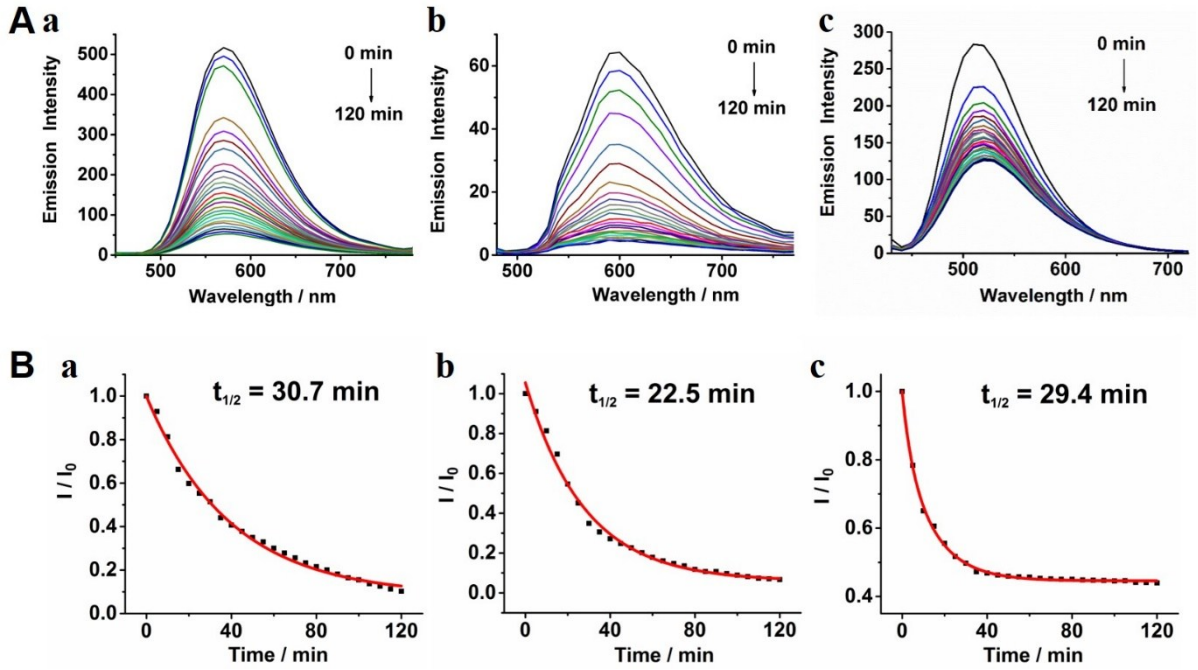

Fig. S13 (A) Time-dependent changes in emission spectra (1×10^{-5} M, λ_{ex} = 405 nm) of **Ir-ART-1** (a), **Ir-ART-2** (b) and **Ir-ART-3** (c) with PLE at 298 K. (B) Plots of relative emission intensities at 570 nm (**Ir-ART-1**, a), 600 nm (**Ir-ART-2**, b) and 520 nm (**Ir-ART-3**, c) versus time of esterase treatment.

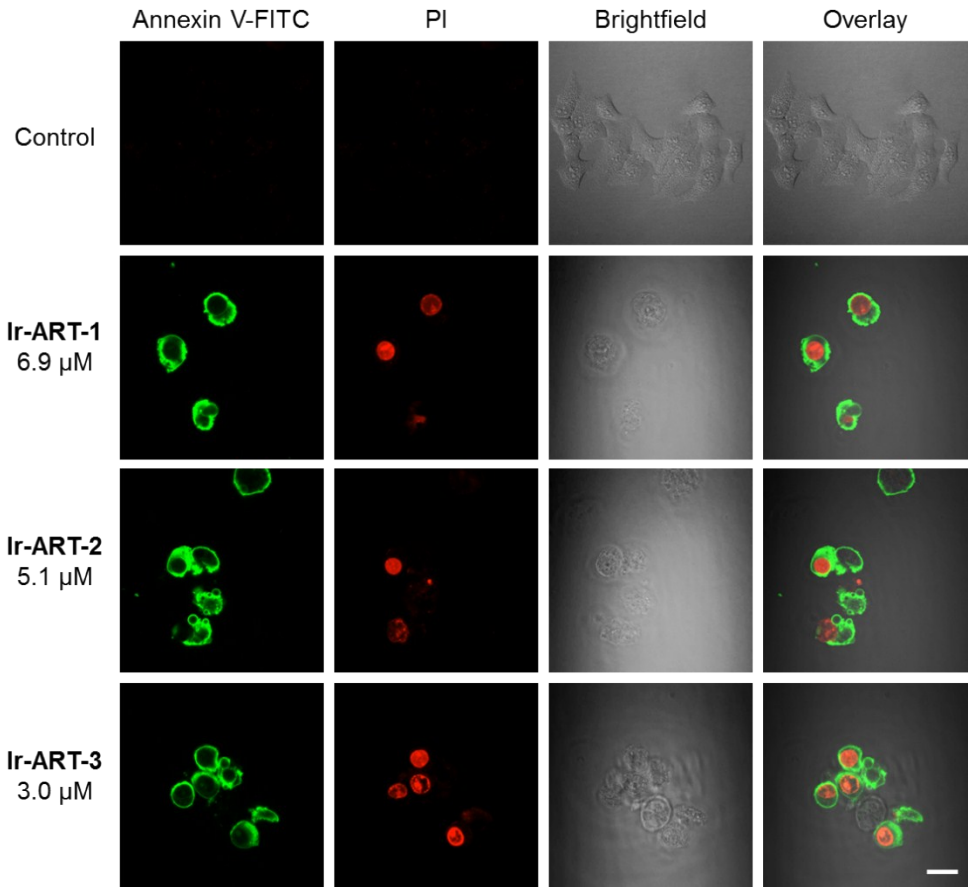

Fig. S14 Detection of apoptosis in HepG2 cells stained with Annexin V-FITC/PI by confocal microscopy after HepG2 cells were incubated with **Ir-ART-1**–**3** for 24 h.

Table S1 Photophysical data of Ir(III) complexes

Compounds	Medium	$\lambda_{abs,\ max}$ (nm)	$\lambda_{em,\ max}$ (nm)
	PBS	380	570
Ir-ART-1	CH_3CN	341	592
	CH_2Cl_2	338	582
	PBS	417	600
Ir-ART-2	CH_3CN	417	615
	CH_2Cl_2	420	605
	PBS	364	520
Ir-ART-3	CH_3CN	362	525
	CH_2Cl_2	365	520
	PBS	380	595
Ir-1	CH_3CN	341	578
	CH_2Cl_2	338	570
	PBS	417	625
Ir-2	CH_3CN	417	590
	CH_2Cl_2	420	590
	PBS	364	533
Ir-3	CH_3CN	362	516
	CH_2Cl_2	365	510

Table S2 Cell-cycle analysis data of Ir(III)-ART conjugates on HepG2 cells[a]

Compounds	G0/G1	S	G2/M
Control	47.17 ± 4.52	38.28 ± 3.81	14.54 ± 1.40
Ir-ART-1 (4.6 μM)	50.39 ± 4.79	26.66 ± 3.00	22.96 ± 2.35
Ir-ART-1 (6.9 μM)	38.15 ± 3.76	22.56 ± 2.30	39.29 ± 3.91
Ir-ART-1 (9.2 μM)	38.90 ± 3.77	25.13 ± 2.55	35.98 ± 3.60
Ir-ART-2 (3.4 μM)	51.75 ± 5.00	24.60 ± 2.78	23.65 ± 2.32
Ir-ART-2 (5.1 μM)	45.85 ± 4.76	26.25 ± 2.88	27.90 ± 2.93
Ir-ART-2 (6.8 μM)	40.72 ± 4.00	25.47 ± 2.55	33.81 ± 3.62
Ir-ART-3 (2.0 μM)	55.91 ± 5.66	26.38 ± 2.68	17.71 ± 1.72
Ir-ART-3 (3.0 μM)	51.92 ± 5.22	25.11 ± 2.54	22.97 ± 2.00
Ir-ART-3 (4.0 μM)	46.36 ± 4.60	25.51 ± 2.46	28.14 ± 2.88

[a] Data shown are mean ± SD of three independent experiments for each treatment.